Nano Research 2013, 6(3): 174–181
DOI 10.1007/s12274-013-0293-y
Research Article

ISSN 1998-0124
CN 11-5974/O4

Scalable preparation of porous silicon nanoparticles and their application for lithium-ion battery anodes

Mingyuan Ge[1], Jiepeng Rong[1], Xin Fang[1], Anyi Zhang[1], Yunhao Lu[2], and Chongwu Zhou[1,3] (✉)

[1] *Department of Chemical Engineering and Materials Science, University of Southern California, 3710 McClintock Ave, Los Angeles, CA 90089, USA*
[2] *Department of Materials Science and Engineering, Zhejiang University, 38 Zheda Road, Hangzhou 310027, China*
[3] *Department of Electrical Engineering, University of Southern California, 3710 McClintock Ave, Los Angeles, CA 90089, USA*

Received: 13 December 2012
Revised: 9 January 2013
Accepted: 10 January 2013

KEYWORDS
porous silicon nanoparticles, scalable production, lithium-ion battery

ABSTRACT

Nanostructured silicon has generated significant excitement for use as the anode material for lithium-ion batteries; however, more effort is needed to produce nanostructured silicon in a scalable fashion and with good performance. Here, we present a direct preparation of porous silicon nanoparticles as a new kind of nanostructured silicon using a novel two-step approach combining controlled boron doping and facile electroless etching. The porous silicon nanoparticles have been successfully used as high performance lithium-ion battery anodes, with capacities around 1,400 mA·h/g achieved at a current rate of 1 A/g, and 1,000 mA·h/g achieved at 2 A/g, and stable operation when combined with reduced graphene oxide and tested over up to 200 cycles. We attribute the overall good performance to the combination of porous silicon that can accommodate large volume change during cycling and provide large surface area accessible to electrolyte, and reduced graphene oxide that can serve as an elastic and electrically conductive matrix for the porous silicon nanoparticles.

1 Introduction

During the last decade, there has been great interest in developing lithium-ion batteries with high energy density and long cycle life to meet the ever increasing demands of portable electronics, implanted medical device, and electric vehicle. However, most of the currently used lithium-ion batteries have suffered from insufficient capacity, mainly due to the low specific capacity of the electrode materials. For example, graphite is a widely used anode with reliable performance; however, the low specific capacity (372 mA·h/g) of graphite has led researchers to seek alternative anode materials with high capacity. Silicon is one of the most promising anode candidates because of its high theoretical capacity of approximately 3,600 mA·h/g at room temperature [1]. However, the drawbacks of silicon anodes are equally obvious. The large volume change during the insertion and extraction of lithium in silicon leads to severe

Address correspondence to chongwuz@usc.edu

pulverization and capacity fading, which has limited the use of silicon in real battery applications. Significant progress has been made of using silicon nanowires [2–5], silicon nanotubes [6, 7], and microporous silicon structures [8–13] as anode materials, and they have shown great promise in overcoming the issues of pulverization and capacity fading. Despite the great achievements, the methods used to grow nanostructured silicon usually require expensive precursors (such as silane [14] and monophenylsilane [15]) and the use of chemical vapor deposition (CVD) or supercritical fluid technique [14, 15]. In parallel, Yushin et al. reported that the cycling performance of silicon nanoparticles can be significantly improved by using a high viscosity binder derived from brown algae synthesized in their own lab [16]. However, the preparation of the binder needs special brown algae as raw material, and might add complexity and expense to lithium-ion battery production. Recently, we have reported that a porous silicon nanowire anode can achieve a capacity of over 1,000 mA·h/g at a current rate of 4 A/g for 2,000 cycles when using commercially available alginate as the binder [12]. We note that while porous silicon nanowires may find broad applications including in lithium-ion batteries, biomedical imaging, and thermoelectric devices [17–19], the preparation of porous silicon nanowires and similar nanostructures is usually achieved by wet etching of doped silicon wafers, and therefore is limited in quantity. A more scalable method is highly desirable for the preparation of porous silicon nanostructures.

Here, we introduce a new and simple synthetic route for the preparation of porous silicon nanoparticles. By doping and then etching of commercially available silicon nanoparticles, porous silicon nanoparticles can be synthesized in bulk quantities. Our approach represents a quantum leap from traditional porous silicon nanowires available only at the surface of etched wafers to novel porous silicon nanoparticles, which can be produced in large quantities and facilitate their use in many applications. For instance, the obtained porous silicon nanoparticles are capable of accommodating large volume change and exhibit impressive performance as lithium-ion battery anodes. We have achieved high specific capacities of 1,400 mA·h/g and 1,000 mA·h/g at current rates of 1.0 A/g and 2.0 A/g with reduced graphene oxide as an additive.

2 Methods

2.1 Synthesis of porous silicon nanoparticles

The synthesis of porous silicon nanoparticles is schematically presented in Fig. 1(a). Silicon nanoparticles with particle size <200 nm (Shanghai Chaowei Nano., Ltd.) were used as starting material. We first doped silicon with boron, and then etched the boron-doped silicon in an etchant containing silver nitrate ($AgNO_3$) and hydrofluoric acid (HF) to obtain a porous structure. In the doping process, typically, 1.0 g of silicon nanoparticles and various amounts of boric acid (0.4 g, 0.8 g, and 1.6 g) were well mixed in solution, and then dried to give a powder which was annealed at 900 °C in an argon environment for three hours. The powder was washed with 5% HF solution and de-ionized water (DI water) to remove byproducts such as B_2O_3 and SiO_2. As obtained boron-doped silicon nanoparticles were then immersed in 50 mL of etchant solution containing 10 mM silver nitrate and 5 M HF under gentle stirring. Immediately, the solution bubbled as an indication of etching. After one hour, reaction was stopped by adding more DI water, and the solution was centrifuged at 8,000 rpm for 10 min, followed by additional washing using DI water. Figure 1(b) shows a photograph of commercial nonporous silicon nanoparticles (left) and porous silicon nanoparticles after the treatment (right). The amount of porous silicon after the treatment is about

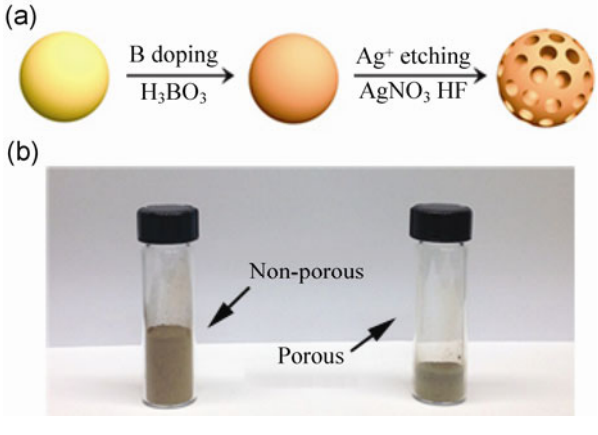

Figure 1 (a) Schematic diagram of the procedure to prepare porous silicon nanoparticles. (b) Photographs of nonporous and porous Si nanoparticles, illustrating the scalable nature of our porous silicon nanoparticle preparation.

1/3 of the original amount of nonporous silicon. We note that this technique is highly scalable to large quantities, as the starting material, silicon nanoparticles, is commercially available in bulk quantities, and the doping and etching processes are also compatible with large-scale manufacturing.

2.2 Measurement of the boron concentration in doped Si nanoparticles

Boron dopant concentration was determined using inductively coupled plasma atomic emission spectrometer (ICP–AES, HORIBA Jobin Yvon ULTIMA-C). Specifically, 0.5 g of a boron-doped silicon sample was put into polytetrafluoroethene (PTFE) beaker containing 5 mL of concentrated nitric acid (HNO_3). 5 mL of 50 wt.% HF was then added dropwise to dissolve sample giving a clear solution. An additional 5 mL of an acid mixture (sulfuric acid (H_2SO_4):phosphoric acid (H_3PO_4) = 3:2) was added and the mixture kept at 130 °C for 5 min. At this stage, all the silicon was converted to silicon tetrafluoride (SiF_4) and removed by volatilization, leaving only boron in the solution. The solution was then cooled down, and diluted with DI water. Standard boric acid (H_3BO_3) solution was used to calibrate the boron concentration. A wavelength of 249.77 nm was selected for the measurements.

2.3 Preparation of porous silicon nanoparticle anodes for lithium-ion batteries

The electrodes were prepared as follows. Porous silicon nanoparticles were first coated with carbon using CVD to help to form a stable solid-electrolyte-interface (SEI) layer during electrochemical tests. In addition, carbon-coated porous silicon nanoparticles were then mixed with reduced graphene oxide (RGO), which can function as an elastic and electrically conductive matrix to hold the particles, and prevent the particles from losing electrical conductivity. Finally, the electrode was prepared from the active material (carbon-coated porous silicon nanoparticles with reduced graphene oxide wrapping, 70%), carbon black (super-P, 20%), and alginic acid sodium salt as binder (10%, Alfa Aesar, denoted as alginate binder), and then assembled in coin cells for further tests.

3 Results and discussion

3.1 Formation of porous silicon nanoparticles

Electroless etching is a versatile method to etch silicon wafers into various kinds of silicon nanostructures (e.g., nanoparticles, nanowires, and porous nanowires) through a galvanic displacement and etching procedure. Here, the mechanism of etching non-porous silicon nanoparticles to porous silicon is similar to the etching of silicon wafers, and includes the following reactions:

$$4Ag^+ + 4e^- \rightarrow 4Ag$$
$$Si + 6F^- \rightarrow [SiF_6]^{2-} + 4e^-$$

In this reaction, silicon donates electrons to reduce Ag^+ to Ag, and simultaneously becomes oxidized and etched away by F^-. Since the redox potential of Ag^+/Ag lies below the valence band of silicon, for p-type silicon (e.g., boron doped silicon nanoparticles as studied here), Ag^+ preferentially reacts with silicon nanoparticles at defect sites (dopant sites), leaving pores on the surface [20].

In order to convert our intrinsic silicon nanoparticles to p-type, we first doped the particles with boron. Figure 2(a) shows TEM images of silicon nanoparticles immediately after the boron doping. There was no significant change of morphology of silicon nanoparticles after boron doping (Fig. 2(a)), and neither second crystal growth, nor particle agglomeration was found. After etching, silicon nanoparticles became porous, as shown in Fig. 2(b), and were surrounded by many Ag nanoparticles (the dark particles shown in Fig. 2(b)) with a broad size distribution from 10–100 nm. These large Ag particles might come from the nucleation and growth of small Ag clusters during the reaction. HNO_3 could be used to remove Ag, leaving neat porous silicon nanoparticles (Fig. 2(c)) with pores with size around 9 nm that are uniformly distributed on top of the particle surface, as shown in Fig. 2(d).

X-ray diffraction (XRD) was used to inspect the purity and crystallographic structure of the intrinsic, doped and etched silicon nanoparticles. As shown in Fig. 3, silicon nanoparticles before etching showed typical silicon diffraction features. After boron doping,

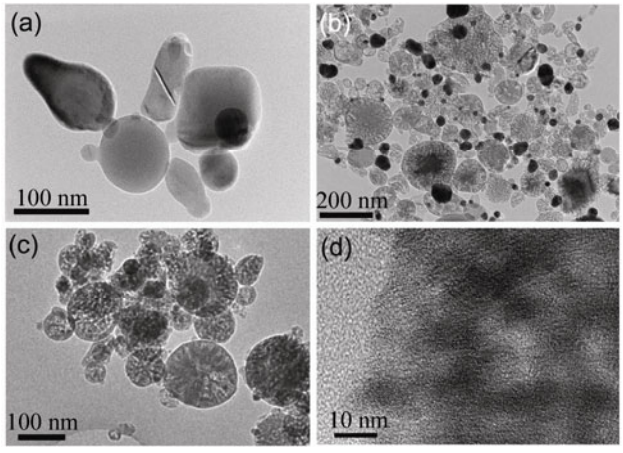

Figure 2 (a) TEM image of silicon nanoparticles after boron doping. (b) TEM image showing porous silicon nanoparticles with large Ag nanoparticles after electroless etching. (c) TEM image of porous Si nanoparticles after washing with HNO_3 and H_2O to remove Ag nanoparticles. (d) High resolution TEM image showing that the pores are uniformly distributed on particle surface with size around 9 nm.

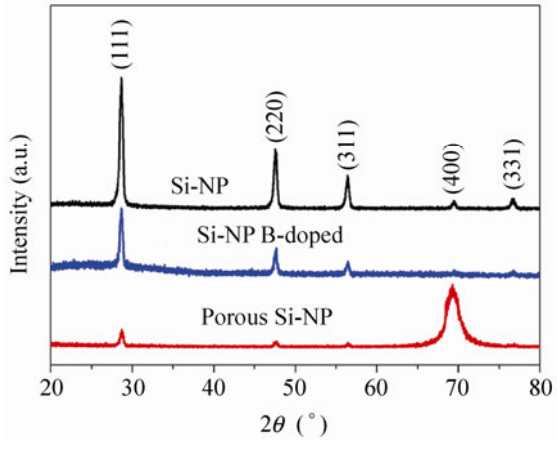

Figure 3 XRD patterns of nonporous Si nanoparticles, boron-doped Si nanoparticles, and porous Si nanoparticles.

the XRD pattern showed a single silicon phase without any sign of Si–B alloy (B_6Si, B_3Si, etc.), demonstrating the successful doping of boron atoms. However, after etching, the red curve in Fig. 3 reveals that the relative intensity ratios of the (400) reflection relative to other reflections were larger than the standard values in the JCPDS card (No. 27-1402), which is indicative of the preferential preservation of (400) planes due to anisotropic etching of Ag^+ along the silicon <100> orientation [21]. Furthermore, detailed analysis of the peak broadening using the Scherrer equation [22] led to a coherence length D_{hkl} for (400) about 26 nm. The small coherence length of (400) compared with the silicon nanoparticle size (~100 nm) confirms the existence of pores in the silicon nanoparticles.

According to the previous analysis, boron doping plays an important role in etching the silicon nanoparticles to give a porous structure; therefore, it is interesting and important to examine the effect of dopant concentration on the final morphology of the porous silicon nanoparticles, since this will provide us with a guideline to synthesize porous silicon nanoparticles with the desired structure. We have observed that the dopant concentration can be well controlled by adjusting the ratio of boric acid to silicon. According to a simplified one-dimensional diffusion model [23]:

$$C(t) = \int C_s \mathrm{erfc}\left(\frac{x}{2\sqrt{Dt}}\right) = \frac{2}{\sqrt{\pi}} C_s \sqrt{Dt}$$

where $C(t)$ is the total boron concentration, C_s is the surface concentration of boron atoms, and D is the diffusion coefficient, a positive correlation between $C(t)$ and C_s is established. In our experiments, three samples with different dopant concentrations were obtained, and characterized by ICP–AES. Figure 4(a) shows that the boron dopant concentration monotonically increases with the increase of initial mass ratio of boric acid to silicon from 2:5 to 8:5. Figures 4(b), 4(c), and 4(d) show the TEM images of porous silicon nanoparticles prepared with initial $Si:H_3BO_3$ mass ratios of 5:2, 5:4, and 5:8, respectively. It is found that silicon nanoparticles with higher doping concentration give rougher surfaces and larger pores after etching (compare Fig. 4(d) with Figs. 4(b) and 4(c)). This phenomenon can be understood by the fact that, higher dopant concentrations in p-type silicon (lower Fermi level) can lower the energy barrier for electron transfer from silicon to Ag, thus facilitating the etching process to generate large pores. The specific surface areas of the porous silicon nanoparticles were analyzed using the Brunauer–Emmett–Teller (BET) method. The surface areas were 61 m^2/g, 69 m^2/g, and 82 m^2/g for porous silicon nanoparticles prepared with initial $Si:H_3BO_3$ mass ratios of 5:2, 5:4, and 5:8, respectively.

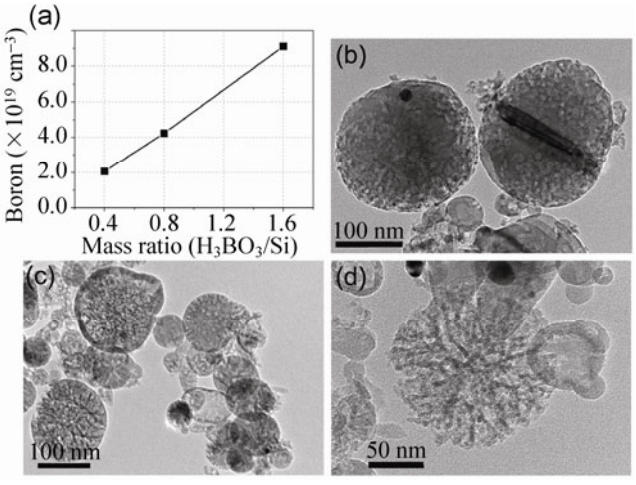

Figure 4 (a) Boron concentration of doped Si nanoparticles prepared using different H_3BO_3:Si mass ratios. TEM images of porous silicon nanoparticles prepared with initial Si:H_3BO_3mass ratios of (b) 5:2, (c) 5:4, and (d) 5:8.

3.2 Test of porous silicon nanoparticles as Li-ion battery anode

Porous silicon nanoparticles are a prospective candidate for lithium-ion battery anodes, as the pores can provide additional space for volume expansion of silicon during the charging process, which will help to retain the structural integrity of silicon and prevent large capacity degradation. Porous silicon nanoparticles were coated with carbon and wrapped with reduced graphene oxide, and then tested as lithium-ion battery anodes.

Figures 5(a) and 5(b) present the measured cyclic voltammograms of porous silicon nanoparticles for the first two cycles. Undoped silicon nanoparticles (coated with carbon, and wrapped with reduced graphene oxide) were also tested as a control to understand the effect of boron doping on the battery voltage. Both curves in Fig. 5(a) show the typical behavior of silicon in the lithiation and delithiation process. The peaks located at 0.5–1.0 V in the charge branch in the first cycle for both doped and undoped silicon nanoparticles are related to the formation of a SEI layer. After the first cycle, as shown in Fig. 5(b), the peak located at 0.2 V in the charge branch in both curves indicates the formation of amorphous silicon.

To obtain a detailed understanding of the effect of boron doping on the battery voltage, differential

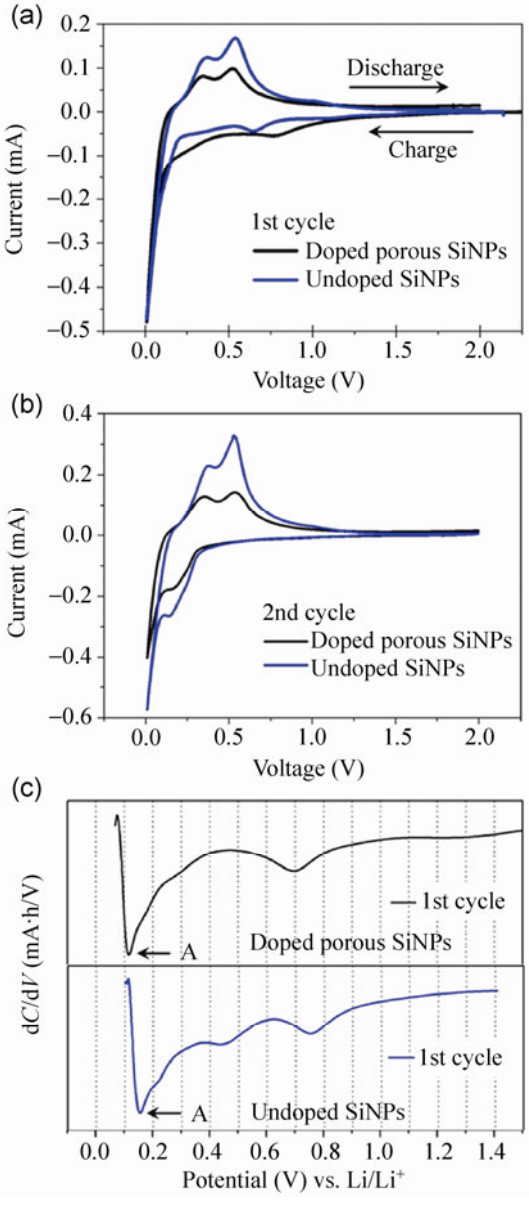

Figure 5 Cyclic voltammograms of doped porous silicon nanoparticles and undoped nonporous silicon nanoparticles for (a) the first cycle and (b) the second cycle. (c) Differential capacity curves of doped porous silicon nanoparticles and undoped nonporous silicon nanoparticles in the charge branch of the first cycle.

capacity was examined as a function of potential for the first cycle and the results are presented in Fig. 5(c). The intercalation voltage, which is related to the lithiation of crystalline silicon (c-Si + nLi → a-Li$_n$Si) [24], is 0.15 V for undoped silicon and 0.12 V for doped porous silicon (Peak A in Fig. 5(c)). The lower intercalation voltage in doped porous silicon might be attributed to the relatively higher conductivity of particles after boron doping, and the relatively lower

intercalation energy of lithium in doped silicon, as we derived from first principles density functional theory (DFT) calculations (see the Electronic Supplementary Material (ESM) for details).

Nevertheless, the difference in intercalation voltage between doped porous silicon nanoparticles and undoped silicon nanoparticles is small. We can therefore conclude that boron doping has no significant effect on the battery working voltage.

The cycling performance of porous silicon nanoparticles as a lithium-ion battery anode is presented in Fig. 6. The voltage range was set to 0.01–2.0 V. The rate performance of porous silicon nanoparticles is demonstrated in Fig. 6(b). It was found that the capacity remained around 2,500, 2,200, 1,400 and 1,000 mA·h/g at current rates of 1/16 C, 1/8 C, 1/4 C, and 1/2 C (1 C = 4 A·h/g), respectively. The high capacity was retained after extended cycling—the capacity remained around 1,400 and 1,000 mA·h/g at 1/4 C and 1/2 C after 200 cycles, as shown in Fig. 6(c). The capacity degradation over 200 cycles is as small as 13% for 1/4 C (from 1,622 mA·h/g for the first few cycles to 1,410 mA·h/g for the 200th cycle), and 19% for 1/2 C (from 1,172 mA·h/g for the first few cycles to 945 mA·h/g for the 200th cycle). Pristine reduced graphene oxide without porous silicon nanoparticles was also tested for comparison, and showed a capacity of less than 100 mA·h/g (see the ESM), and therefore made only a minor contribution to the overall capacity.

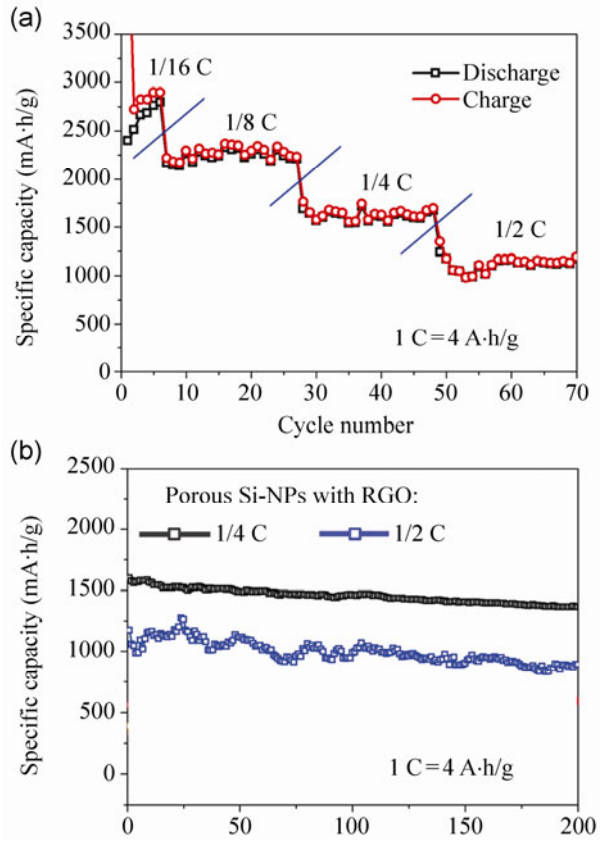

Figure 6 Characterization of porous silicon nanoparticles with carbon coating and reduced graphene oxide wrapping as lithium-ion battery anodes: (a) charge/discharge capacity at current rates of 1/16 C, 1/8 C, 1/4 C, and 1/2 C, (1 C = 4 A·h/g); (b) cycling performance at current rates of 1/4 C and 1/2 C.

The performance of our graphene-wrapped porous silicon nanoparticle anode compares favorably with results in recent publications. For instance, Lee et al. reported using nonporous silicon nanoparticle/graphene composites as lithium-ion battery anodes [25]; however, their anodes exhibited a significant capacity degradation of around 47% at 1/4 C (from ~1,900 mA·h/g for the first few cycles to ~1,000 mA·h/g after 120 cycles). In comparison, our graphene-wrapped porous silicon nanoparticle anodes exhibited much better cyclability and much less capacity degradation. In addition, Liu et al. used porous silicon particles without a graphene wrapping and achieved an anode capacity of 2,826 mA·h/g for the first cycle and 1,022 mA·h/g for the 50th cycle at a relatively low charging rate of 1/10 C [26]. In comparison, our anodes are able to operate at much higher current rates of 1/4 C and 1/2 C, and have delivered very stable capacity of 1,400 and 1,000 mA·h/g after 200 cycles. We attribute the enhanced rate performance and cyclability of our anodes to the structure of the graphene-wrapped porous silicon nanoparticles, as porous silicon nanoparticles can accommodate large volume changes during cycling and offer a large surface area accessible to the electrolyte, while the reduced graphene oxide wrapping can serve as an elastic and electrically conductive matrix, and therefore boost the overall battery performance.

4 Conclusions

We have reported a facile doping and electroless etching method to prepare porous silicon nanoparticles using silicon nanoparticles that are available in bulk

quantities as a starting material. We have shown that the porous silicon nanoparticles are a potential anode material for lithium-ion batteries. Our battery tests have demonstrated that porous silicon nanoparticle anodes are able to deliver capacities around 1,400 mA·h/g and 1,000 mA·h/g at current rates of 1/4 C and 1/2 C, respectively, and show stable operation up to 200 cycles. The scalable and cost-efficient preparation method we have reported may stimulate further study of the fundamental properties of porous silicon nanoparticles, and the materials may find broad applications for lithium-ion batteries, biomedical imaging, and thermoelectric devices.

Acknowledgements

This work was supported by University of Southern California. This work was also supported by High-Performance Computing and Communications at University of Southern California.

Electronic Supplementary Material: Supplementary material (first principles calculation of Li intercalation voltage in boron-doped silicon, TEM image of porous silicon nanoparticles with carbon coating and graphene wrapping, cycling performance of pristine reduced graphene oxide, improved first cycle Coulombic efficiency by pre-lithiation of porous silicon nanoparticles) is available in the online version of this article at http://dx.doi.org/10.1007/s12274-013-0293-y.

References

[1] Obrovac, M. N.; Christensen, L. Structural changes in silicon anodes during lithium insertion/extraction. *Electrochim. Solid-State Lett.* **2004**, *7*, A93–A96.

[2] Zhou, S.; Liu, X. H.; Liu, Wang, D. W. Si/$TiSi_2$ heteronanostructures as high-capacity anode material for Li ion batteries. *Nano Lett.* **2010**, *10*, 860–863.

[3] Peng, K. Q.; Jie, J. S.; Zhang, W. J.; Lee, S. T. Silicon nanowires for rechargeable lithium-ion battery anodes. *Appl. Phys. Lett.* **2008**, *93*, 033105.

[4] Chan, C. K.; Patel, R. N.; O'Connell, M. J.; Korgel, B. A.; Cui, Y. Solution-grown silicon nanowires for lithium-ion battery anodes. *ACS Nano* **2010**, *4,* 1443–1450.

[5] Chan, C. K.; Peng, H. L.; Liu G.; McIlwrath, K.; Zhang, X. F.; Huggins, R. A.; Cui, Y. High-performance lithium battery anodes using silicon nanowires. *Nat. Nanotechnol.* **2008**, *3*, 31–35.

[6] Park, M.-H.; Kim, M. G.; Joo, J.; Kim, K.; Kim, J.; Ahn, S.; Cui, Y.; Cho, J. Silicon nanotube battery anodes. *Nano Lett.* **2009**, *9*, 3844–3847.

[7] Song, T.; Xia, J. L.; Lee, J.-H.; Lee, D. H.; Kwon, M.-S.; Choi, J.-M.; Wu, J.; Doo, S. K.; Chang, H.; Park, W.; et al. Arrays of sealed silicon nanotubes as anodes for lithium ion batteries. *Nano Lett.* **2010**, *10*, 1710–1716.

[8] Qu, Y. Q.; Liao, L.; Li, Y. J.; Zhang, H.; Huang, Y.; Duan, X. F. Electrically conductive and optically active porous silicon nanowires. *Nano Lett.* **2009**, *9*, 4539–4543.

[9] Magasinski, A.; Dixon, P.; Hertzberg, B.; Kvit, A.; Ayala, J.; Yushin, G. High-performance lithium-ion anodes using a hierarchical bottom-up approach. *Nat. Mater.* **2010**, *9*, 353–358.

[10] Kim, H.; Han, B.; Choo, J.; Cho, J. Three-dimensional porous silicon particles for use in high-performance lithium secondary batteries. *Angew. Chem. Int. Ed.* **2008**, *47*, 10151–10154.

[11] Yao, Y.; McDowell, M. T.; Ryu, I.; Wu, H.; Liu, N. A.; Hu, L. B.; Nix, W. D.; Cui, Y. Interconnected silicon hollow nanospheres for lithium-ion battery anodes with long cycle life. *Nano Lett.* **2011**, *11*, 2949–2954.

[12] Ge, M.; Rong, J.; Fang, X.; Zhou, C. Porous doped silicon nanowires for lithium ion battery anode with long cycle life. *Nano Lett.* **2012**, *12*, 2318–2323.

[13] Chen, X. L.; Gerasopoulos, K.; Guo, J. C.; Brown, A.; Ghodssi, R.; Culver, J. N.; Wang, C. S. High rate performance of virus enabled 3D n-type Si anodes for lithium-ion batteries. *Electrochim. Acta* **2011**, *56*, 5210–5213.

[14] Lu, X. M.; Hanrath, T.; Johnston, K. P.; Korgel, B. A. Growth of single crystal silicon nanowires in supercritical solution from tethered gold particles on a silicon substrate. *Nano Lett.* **2003**, *3*, 93–99.

[15] Holmes, J. D.; Johnston, K. P.; Doty, R. C.; Korgel, B. A. Control of thickness and orientation of solution-grown silicon nanowires. *Science* **2000**, *287*, 1471–1473.

[16] Kovalenko, I.; Zdyrko, B.; Magasinski, A.; Hertzberg, B.; Milicev, Z.; Burtovyy, R.; Luzinov, I.; Yushin, G. A major constituent of brown algae for use in high-capacity Li-ion batteries. *Science* **2011**, *334,* 75–79.

[17] Lin, V. S.-Y.; Motesharei, K.; Dancil, K. P. S.; Sailor, M. J.; Ghadiri, M. R. A porous silicon-based optical interferometric biosensor. *Science* **1997**, *278*, 840–843.

[18] Hochbaum, A. I.; Gargas, D.; Hwang, Y. J.; Yang, P. D. Single crystalline mesoporous silicon nanowires. *Nano Lett.* **2009**, *9*, 3550–3554.

[19] Tang, J. Y.; Wang, H.-T.; Lee, D. H.; Fardy, M.; Huo, Z.; Russell, T. P.; Yang, P. D. Holey silicon as an efficient thermoelectric material. *Nano Lett.* **2010**, *10*, 4279–4283.

[20] Peng, K. Q.; Hu, J. J.; Yan, Y. J.; Wu, Y.; Fang, H.; Xu, Y.; Lee, S.-T.; Zhu, J. Fabrication of single-crystalline silicon nanowires by scratching a silicon surface with catalytic metal particles. *Adv. Funct. Mater.* **2006**, *16*, 387–394.

[21] Peng, K.; Lu, A.; Zhang, R.; Lee, S. Motility of metal nanoparticles in silicon and induced anisotropic silicon etching. *Adv. Funct. Mater.* **2008**, *18*, 3026–3035.

[22] Patterson, A. L. The Scherrer formula for X-ray particle size determination. *Phys. Rev.* **1939**, *56*, 978–982.

[23] Silva, J. A.; Brito, M. C.; Costa, I.; Alves, J. M.; Serra, J. M.; Vallêra, A. M. Sprayed boric acid as a dopant source for silicon ribbons. *Sol. Energy Mater. Sol. Cells* **2007**, *91*, 1948–1953.

[24] Chan, C. K.; Ruffo, R.; Hong, S. S.; Huggins, R. A.; Cui, Y. Structural and electrochemical study of the reaction of lithium with silicon nanowires. *J. Power Sources* **2009**, *189*, 34–39.

[25] Lee, J. K.; Smith, K. B.; Hayner, C. M.; Kung, H. H. Silicon nanoparticles–graphene paper composites for Li ion battery anodes. *Chem. Commun.* **2010**, *46*, 2025–2027.

[26] Liu, Y.; Chen, B.; Cao, F.; Chen, H. L. W.; Zhao, X.; Yuan, J. One-pot synthesis of three-dimensional silver-embedded porous silicon micronparticles for lithium-ion batteries. *J. Mater. Chem.* **2011**, *21*, 17083–17086.